THE SOUTH SANDWICH ISLANDS EARTHQUAKE OF 27 JUNE 1929: SEISMOLOGICAL STUDY AND INFERENCE ON TSUNAMI RISK FOR THE SOUTH ATLANTIC

E.A. OKAL

Department of Earth and Planetary Sciences, Northwestern University, Evanston, IL 60208, United States of America
e-mail: emile@earth.northwestern.edu

C.J. HARTNADY

UMVOTO Pty. Limited, Post Office Box 61, Muizenberg, 7950, Cape Provence, South Africa
e-mail: chris@umvoto.com

ABSTRACT

While no large interplate thrust earthquakes are known at the South Sandwich subduction zone, historical catalogues include a number of earthquakes with reported magnitudes of 7 or more. We present a detailed seismological study of the largest one (27 June 1929; M_{PAS} = 8.3). The earthquake relocates 80 km north of the north-western corner of the arc. Its mechanism, inverted through the PDFM method, features normal faulting on a steeply dipping fault plane (φ = 71°, δ = 70°, λ = 272°). The seismic moment, 1.7 x 10^{28} dyn.cm, supports Gutenberg and Richter's estimate, and is 28 times the largest shallow CMT in the region. The 1929 event is interpreted as representing a lateral tear in the South Atlantic plate, comparable to similar earthquakes in Samoa and Loyalty, deemed "STEP faults" by Govers and Wortel (2005). Hydrodynamic simulations using the MOST method (Titov and Synolakis, 1997) suggest deep-water tsunami amplitudes reaching 30 cm off the coast of Brazil, where run-up should have been observable, and 20 cm along the Gulf of Guinea (Ivory Coast, Ghana). We also simulate a number of potential sources obtained by assigning the 1929 moment to the geometries of other known earthquakes in the region, namely outer-rise normal faulting events at the center of the arc and its southern extremity, and an interplate thrust fault at the southern corner, where the youngest lithosphere is subducted. A common feature of these models is the strong focusing of tsunami waves by the South Atlantic Ridge, the southwest Indian Ocean Ridge, and the Agulhas Rise, resulting in amplitudes always enhanced in Ghana, southern Mozambique and certain parts of the coast of South Africa. This study documents the potential tsunami hazard to South Atlantic shorelines from earthquakes in this region, principally normal faulting events.
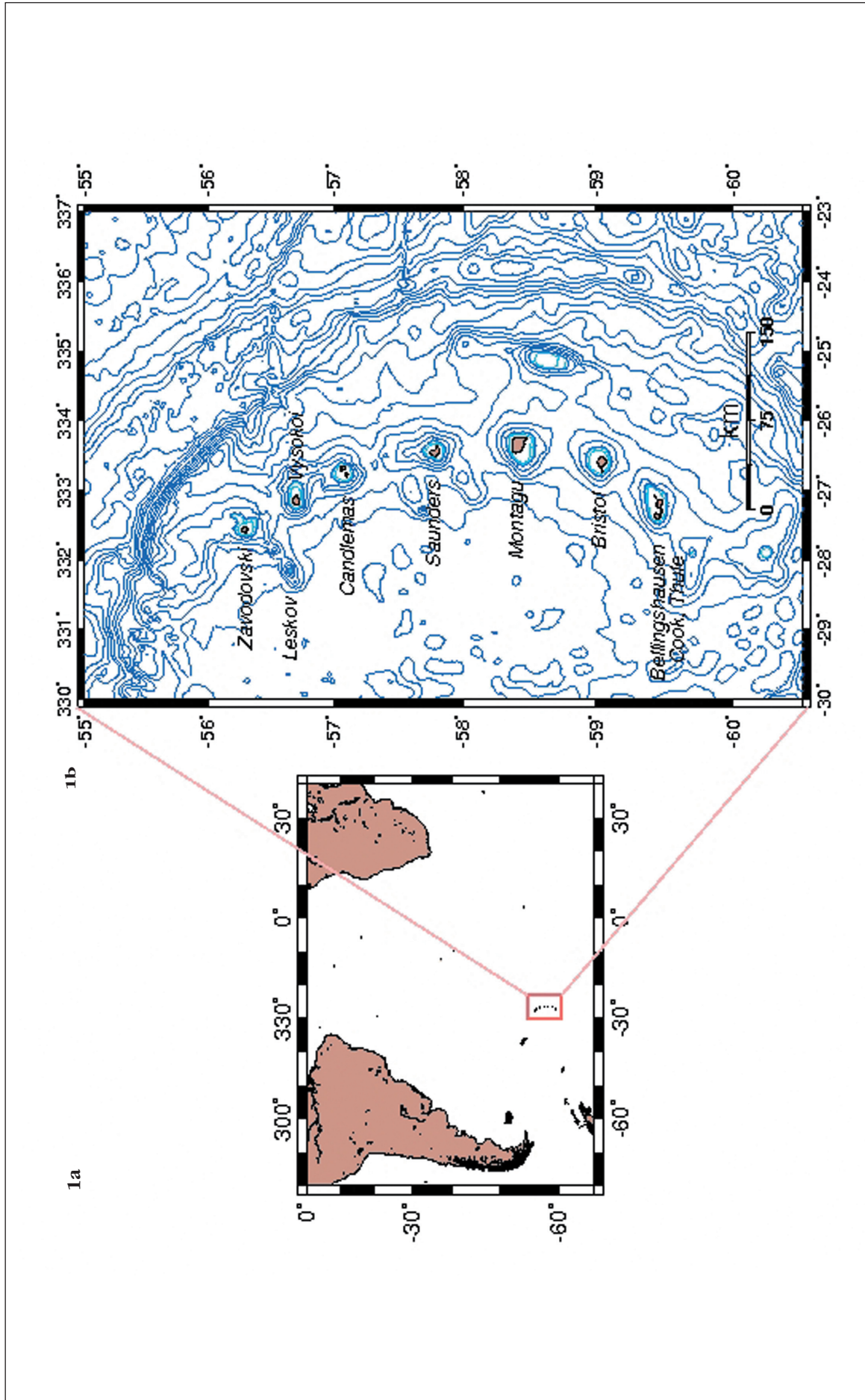
Introduction

The catastrophic Sumatra earthquake of 26 December 2004 has reawakened, in the scientific community, the awareness of tsunami risk in the Indian Ocean, and in particular on the coasts of South Africa. While its tsunami had limited effect on South African coasts, the area of Port Elizabeth did suffer two confirmed casualties by drowning, and minor damage in the harbour, where the run-up reached 2.1 m (Hartnady and Okal, 2008). This moderate level of flooding was the result of a fortunate combination of circumstances, namely the arrival of the tsunami at low tide and an unfavourable directivity effect at the source. In particular, Okal and Synolakis (2008) have documented a number of scenarios of mega-earthquakes at other subduction zones of the Indian Ocean, under which tsunamis of significantly greater amplitude than in 2004 could attack South Africa.

Another subduction zone worthy of attention is the 400 km long South Sandwich Islands (SSI) arc, located at the southern extremity of the South Atlantic (Figure 1), less than 5000 km from South Africa, and where oceanic lithosphere from the South American plate subducts under the small Scotia plate along a trench totalling 700 km in length. Together with the Caribbean system in the north, the Scotia system may be related to the lateral escape of asthenospheric flow around the continent of South America, as the Nazca-South American subduction recesses oceanwards due to the westwards absolute motion of the South American plate (Alvarez, 1982; Russo and Silver, 1996).

While the similitude between the Caribbean and Scotia systems has long been noticed (Wilson, 1966), significant differences exist between the two, most notably the existence of a fully developed back-arc spreading system in Scotia (Barker, 1972). A more trivial difference is that the South Sandwich Islands remain uninhabited and of considerably more difficult access than their Caribbean counterparts, resulting in only fragmentary knowledge of the geological properties of these comparatively small edifices (Baker, 1990), and hence of the tectonic processes at the South Sandwich subduction zone.

In addition, the presence of the long Conrad Fracture Zone (Sclater et al., 1976) leads to a strong discontinuity in age (and presumably in thermal regime) in the lithosphere being subducted at the South Sandwich arc, with ages of 60 to 80 Ma north of 58°S, but less

Figure 1. (**a**) General location map of the South Atlantic, showing the South Sandwich Island Arc. (**b**) Close-up of the box below as marked (**a**), identifying the islands by name, in relation to the trench. Bathymetric contours are at 500 m intervals.

Table 1. Relocations of the main shock (M) and associated events

Number	Date D M (J) Y	Origin Time GMT	Latitude °S	Longitude °W	Number of phases	r.m.s. (s)	Magnitude PAS (GandR)
Main Shock							
M	27 June (178) 1929	12:47:20.2	54.53	29.54	22	3.7	8.3
Fore- and After-shocks							
1	28 March (087) 1929	20:18:05.5	54.76	28.75	12	3.4	$6^{1/2}$
2	27 June (178) 1929	15:17:10			6		
3	02 July (183) 1929	15:11:54			4		
4	02 October (275) 1929	09:18:07.0	56.17	30.39	6	2.3	
5	06 December (340) 1929	16:46:50.9	52.70	27.34	11	3.4	$6^{3/4}$
6	06 December ((340) 1929	20:21:10.8	54.46	28.90	13	3.7	$6^{3/4}$
7	30 March (089) 1930	08:26:06.8	54.98	28.75	12	3.9	$6^{3/4}$
8	21 April (111) 1930	11:50:53.2	55.91	25.44	11	3.9	$6^{3/4}$
9	19 May (139) 1930	03:11:55.1	56.89	26.33	7	4.8	
10	18 August (220) 1930	09:53:41.2	54.87	26.85	23	4.9	7.1
Auxiliary Events							
A	13 September (256) 1921	02:36:55.8	55.18	28.45	8	3.9	7.2
B	28 February (049) 1949	00:13:13.3	55.29	30.11	19	4.3	7.0

than ~20 Ma to the south (Larson et al., 1985). This could lead to a fragmentation of the subduction process along the arc.

From the seismological standpoint, the SSI are remarkably deprived of great interplate thrust earthquakes. The largest such event documented in the CMT catalogue occurred on 30 January 1987 at the extreme southern end of the arc (60.7°S; 26.8°W), with a moment of only 3.3 x 10^{26} dyn.cm. The only larger events in the catalogue are normal faulting outer rise earthquakes (e.g. 27 December 1991; M_0 = 6.0 x 10^{26} dyn.cm). While this situation is somewhat reminiscent of the Greater Antilles, it is unparalleled for a subduction system involving lithosphere as young as found in the southern section of the SSI arc. However, large intermediate-depth earthquakes tend to occur regularly in the SSI arc; notable among them are the doublets on 01 and 08 September 1961 ($h \approx$ 130 km; M_0 = 1.2 and 0.6 x 10^{27} dyn.cm, respectively (Okal, 1992)) and the large 1964 event (h = 120 km; M_0 = 6.2 x 10^{27} dyn.cm (Abe, 1972)).
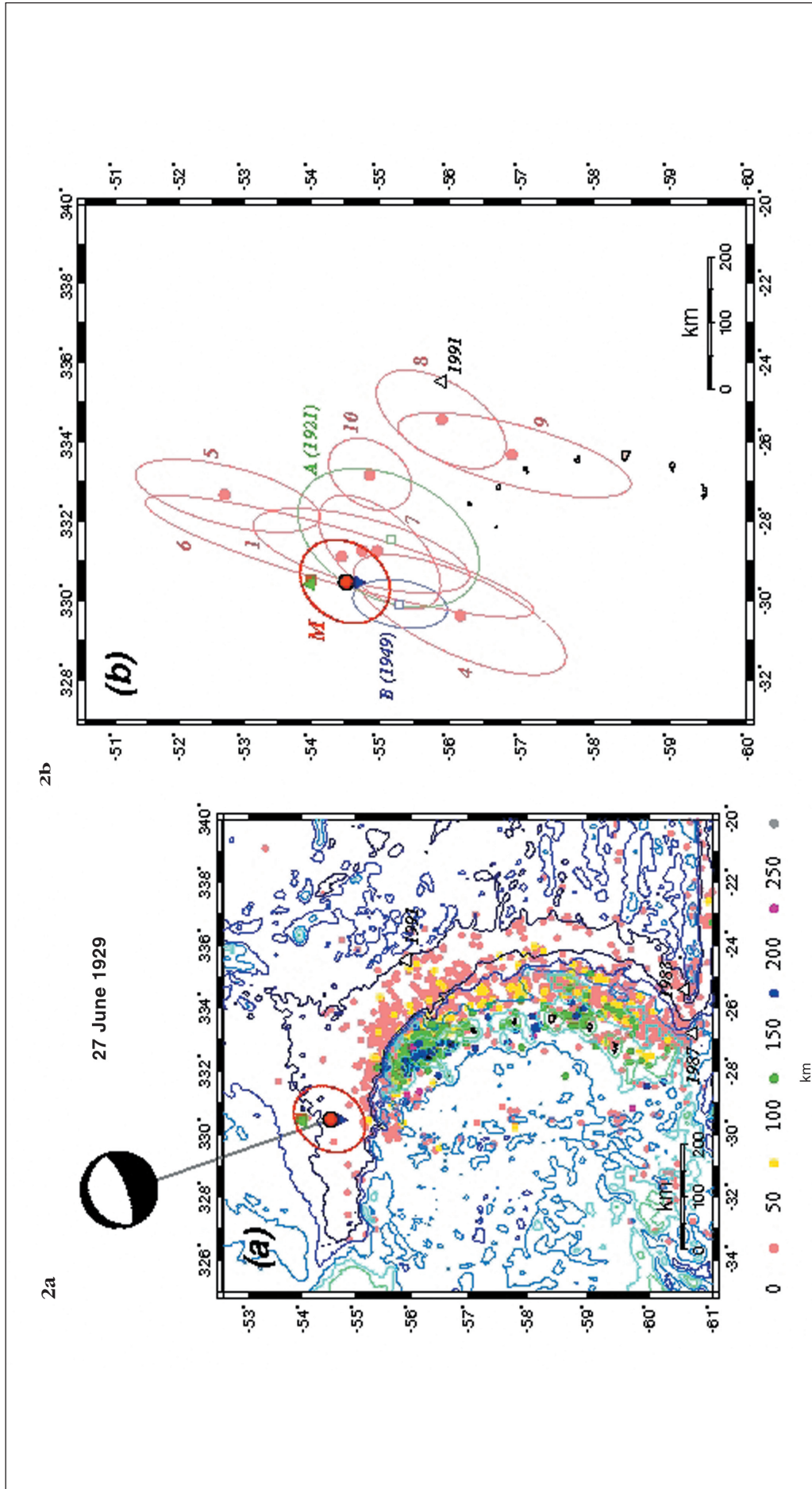
By contrast, in the instrumental historical period (1900 to 1962), eight shallow earthquakes ($h \leq$ 70 km) are documented with a magnitude greater than 7 (Gutenberg and Richter, 1954), which clearly shows that the recent digital era undersamples the true potential of the region for large earthquakes. In particular, the largest historical event documented in the South Sandwich region occurred on 27 June 1929, was located at the north-western corner of the subduction system, and was assigned a magnitude of 8.3 by Gutenberg and Richter (1954); such estimates are reported as M_{PAS} (for "Pasadena") in the historical catalogues compiled by the United States Geological Survey. A large earthquake (M_{PAS} = 7.2) also took place in its vicinity on 13 September 1921.

While the absence of documented large thrust earthquakes at the subduction interface would be supported by the absence of any reports of elevated terraces on the islands, the lack of detailed geological mapping leaves open, at least in principle, the possibility of such events occurring too rarely to be represented in the modern seismological record. In this respect, it is important to reassess the largest events recorded historically, in order to put constraints on their depths, focal mechanisms, and moments, and on their capacity to generate tsunamis potentially destructive in the far field. We present here a detailed seismological investigation of the earthquake of 27 June 1929.

Relocation

We relocated the 1929 event based on arrival times listed in the International Seismological Summary (ISS), and using the iterative interactive technique of Wysession et al. (1991), which evaluates the quality of the solution through a Monte Carlo algorithm injecting Gaussian noise (σ_G = 6 s for an event in the late 1920s) into the dataset. We retained P times from 22 stations at distances of 28° to 100°. Unfortunately, the dataset cannot resolve depth, as most stations are located beyond 30°. As a result, the depth was constrained at 25 km during the relocation; we verified that the epicenter is robust with respect to a variation in constrained depth. As shown on Figure 2a, the relocation converges on (54.53°S; 29.54°W), with the Monte Carlo ellipse barely reaching the zone of intense seismicity defining the plate boundary, at the extreme north-western end of the arc.

This relocated epicentre is situated 59 km south of both the ISS epicentre (54°S; 29.6°W) and Gutenberg and Richter's (1954) solution (54°S; 29.5°W), and 20 km north of Engdahl and Villaseñor's (2002) relocation (54.71°S; 29.55°W), the latter using a fixed depth of

Figure 2. (***a***) *Background seismicity of the South Sandwich arc province, defined as NEIC epicenters (1963 to 2007) with at least one magnitude > 4, and color-coded by depth. Superimposed is our relocation of the 1929 main shock (large solid dot) with 95%-confidence ellipse. The epicenters determined by the ISS, Gutenberg and Richter (1954), and Engdahl and Villaseñor (2002) are shown by the solid triangle, square, and inverted triangle, respectively. The large events in 1983, 1987 and 1991 are shown for reference, as open triangles. The beachball shows the mechanism inverted in Section 3.*
(***b***) *Relocation of main shock, fore- and after-shocks and relevant events. The main shock (M) is shown as the red dot circled in black, with its 95%-confidence ellipse in red.*
The other relocatable events are shown in pink, and labeled according to Table 1. Also shown (open squares) are the probably independent events of 1921 (A) in green and 1949 (B) in blue. For reference, the largest shallow event in the modern digital era is shown as the open triangle (1991).

Table 2. Seismic records used in this study

Code	Name	Distance (°)	Azimuth (°)	Back-Azimuth (°)	Instrument and Component	Phases used
LPZ	La Paz, Bolivia	48.18	306.6	150.8	Bifilar NS	P
PAR	Paris St. Maur, France	106.62	21.5	198.9	Wiechert EW	G_1
PAR	Paris St. Maur, France	106.62	21.5	198.9	Golytsin Z	$Pdiff$
RIV	Riverview, New South Wales, Australia	91.82	180.6	179.6	Wiechert EW	G_1
RIV	Riverview, New South Wales, Australia	91.82	180.6	179.6	Wiechert NS	R_1
TUC	Tucson, Arizona	111.03	296.1	141.8	Wood-Anderson NS	G_1, R_1
WEL	Wellington, New Zealand	296.1	198.2	166.0	Milne-Shaw EW	G_1
WEL	Wellington, New Zealand	82.14	198.2	166.0	Milne-Shaw NS	R_1

35 km. Our Monte Carlo ellipse includes all three published locations.

By itself, this relocation of the 1929 event suggests that it is an intraplate earthquake occurring in the lithosphere of the South American plate, rather than an interplate thrust event or an event inside the subducting slab, and thus justifies our choice of a shallow constrained depth.

We also selected for relocation a number of events which could be considered foreshocks or aftershocks of the 1929 main shock, namely all shocks occurring between January 1929 and December 1930, with initial locations (ISS or Gutenberg and Richter) west of 27°W.

Of the ten such earthquakes, listed in Table 1 and shown on Figure 2b, Event 2 (apparently an immediate aftershock), recorded at only three stations, could not be relocated, and Event 3 (with only four usable phases listed) is compatible with the main shock's epicenter (the r.m.s. residual being only 2.2 s), but cannot be meaningfully relocated. Events 1 (a possible foreshock), 4, 6, and 7 have Monte Carlo ellipses intersecting that of the main shock, and Event 5 relocates 250 km to the northeast, but with a Monte Carlo ellipse approaching within 40 km of that of the main shock. Similarly, Event 10 relocates 200 km east of the main shock, with a gap of about 80 km between their confidence ellipses. On the other hand, Event 8 relocates as an outer rise earthquake, 269 km from the main shock in the area of the large 1991 normal faulting shock (open triangle on Figure 2b), and as such is probably unrelated to the 1929 main shock. As for Event 9, it could be either inter- or intra-plate, but again is sufficiently removed (336 km) from the 1929 main shock to be considered unrelated to its rupture. We also relocated the two large earthquakes of 13 September 1921 and 28 February 1949 (open squares on Figure 2b), whose epicenters are indistinguishable from that of the 1929 main shock, thus suggesting a sustained level of seismicity in the area, despite an apparent episode of relative quiescence since the onset of modern global instrumentation in 1963.

In conclusion, our relocations confirm that the main shock was accompanied by one possible foreshock and a significant series of aftershocks, lasting for several months, and if Events 5 and 10 are interpreted as aftershocks occurring on the fault plane, they would suggest a fault length of at least 100 km.
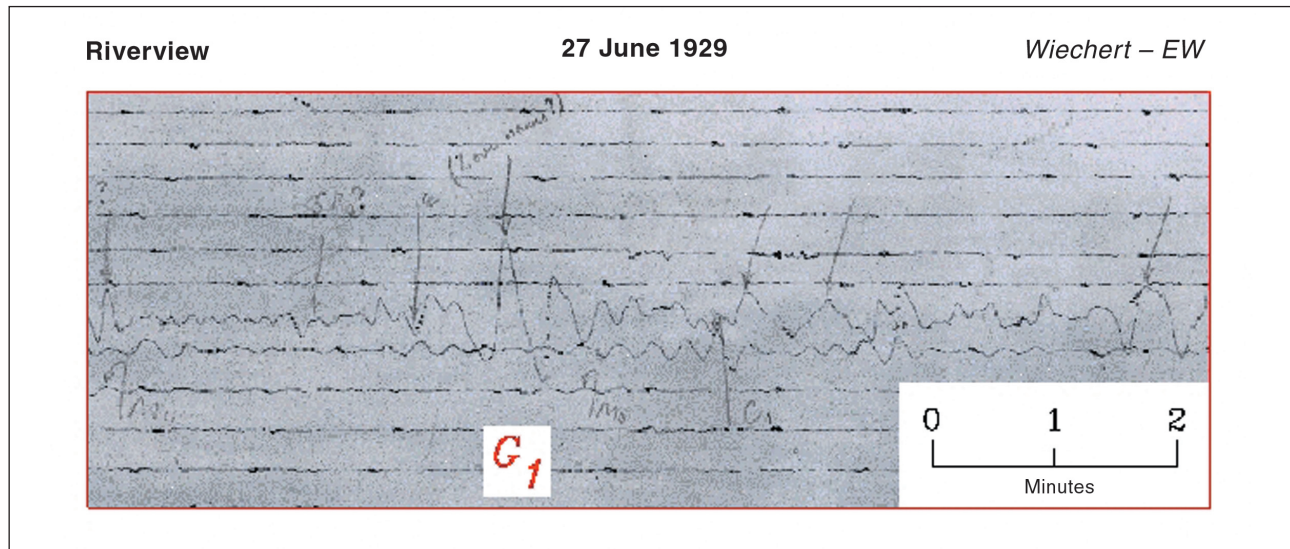
Focal mechanism and seismic moment

Table 2 lists historical seismograms of the 1929 event that we were able to copy or scan at various archival centers. For the purpose of inverting a moment tensor, we focused on hand-digitised records of mantle surface waves G_1 (Love) and R_1 (Rayleigh), and used the mantle magnitude algorithm introduced by Okal and Talandier (1989) to compute a dataset of spectral amplitudes for frequencies ranging from 5 to 10 mHz. In turn, those were inverted into a moment tensor solution using the PDFM technique (Preliminary Determination of Focal Mechanism) introduced by Reymond and Okal (2000). Because this technique inverts only spectral amplitudes and discards the phase information, it is particularly suited to historical events for which both an inaccurate source location or unsuspected timing errors could significantly affect the inversion of spectral phases. Okal and Reymond (2003) and Okal (2005) have demonstrated that the PDFM method can be applied successfully on datasets of as few as three stations well distributed in azimuth. However, as initially pointed out by Romanowicz and Suárez (1983), the method suffers from a double indeterminacy of ± 180° on both the strike and slip angles of the mechanism, which needs to be resolved by independent observations, such as the polarity of a critical set of first arrival P waves.

Our dataset consists of Love and Rayleigh waves at Tucson, Arizona (TUC); Riverview, New South Wales (RIV; Figure 3); and Wellington, New Zealand (WEL), and Love waves at Paris-Saint Maur, France (PAR). Figure 4 shows the result of the inversion with the four possible solutions outlined at right. The normal faulting nature of the event is constrained by the record of the P arrival at La Paz, Bolivia (LPZ) which clearly indicates a component of first motion to the south, i.e., "kataseismic" or back towards the source; similarly, the P_{diff} arrival at PAR is emergent kataseismic. This combination resolves the double indeterminacy in favor of mechanism I:

$$(\varphi=71°; \ \delta=70°; \ \lambda = 272°).$$

Figure 4 further shows that the quality of the inversion is optimised for a centroid depth of 25 km; while a secondary minimum is present around 50 km, we do not favour it in the case of an intraplate earthquake.

Figure 3. *Example of record used in the PDFM inversion: East-West record of the Wiechert instrument at Riverview. Note the strong Love arrival (G_1) on this perfectly polarized station (back-azimuth β = 179.6°).*

The inverted seismic moment, M_0 = 1.7 x 10^{28} dyn.cm, is 25 times that the largest published CMT solution in the region, the 1991 outer rise event. It confirms both the exceptional character of the 1929 earthquake, and the under-representation of the true level of seismicity in the South Sandwich Islands by the seismic record of the past 30 years. Scaling laws (Geller, 1976) applied to this moment value suggest a fault length of ~130 km, consistent with the results of our relocations.

From the standpoint of its focal geometry, the earthquake is characterised by a sub-horizontal T axis oriented N159°E, only 15° away from the local direction to the pole of rotation of the East Scotia and South American plates (Thomas et al., 2003). In this respect, it is reminiscent of earthquakes with similar geometries around the Samoa corner at the extremity of the Tonga arc (e.g., 24 December 1992), at the junction of the Vanuatu arc with the Hunter transform fault (e.g., 16 May 1995), or around the Calabrian arc (Irpinia, 23 November 1980) (Bernard and Zollo, 1989; Pelletier et al., 1998; Millen and Hamburger, 1998). Such events involve a tear in the plate (Isacks et al., 1969; Forsyth, 1975), that separates its subducting segment along a so-called Subduction-Transform Edge Propagator (STEP) fault (Govers and Wortel, 2005); the 1929 earthquake underlines their existence along the South Sandwich arc, and documents the fact they can reach a very substantial size.

Tsunami simulations

At the level of seismic moment inverted above, the 1929 event almost certainly generated a local tsunami, whose waves could also have been recorded at teleseismic distances, given favorable propagation conditions. In this context, we conducted a simulation of that probable tsunami, using the MOST code (Titov and Synolakis, 1997), which solves the non-linear equations of hydrodynamics under the shallow-water approximation, using a finite difference scheme and the method of fractional integration steps (Godunov, 1959). Full details are given in Synolakis (2002). Starting with the value M_0 = 1.7 x 10^{28} dyn.cm, we use scaling laws (Geller, 1976) to obtain the following estimates of source parameters: fault length L = 133 km, fault width W = 66 km, seismic slip Δu = 3.9 m. Note that L is in general agreement with the possible extent of aftershocks as suggested by Figure 2b. We then use the algorithm of Mansinha and Smylie (1971) to map the static displacement of the ocean floor using the simplified model of a homogeneous half-space. In turn, its vertical amplitude (with a maximum value of -1.57 m) is taken as the field of initial displacement η(t = 0_+) of the ocean surface which, together with a condition of zero depth-averaged fluid velocity, forms the initial conditions of the simulation. This approximation is classically used and reasonable as long as the earthquake rupture can be considered as instantaneous with respect to the evolution of the tsunami, which is justified since earthquake rupture velocities (> 1 km/s even for the slowest seismic events) are always much greater than those of tsunami waves (typically 220 m/s on the high seas; less over shallow bathymetry).
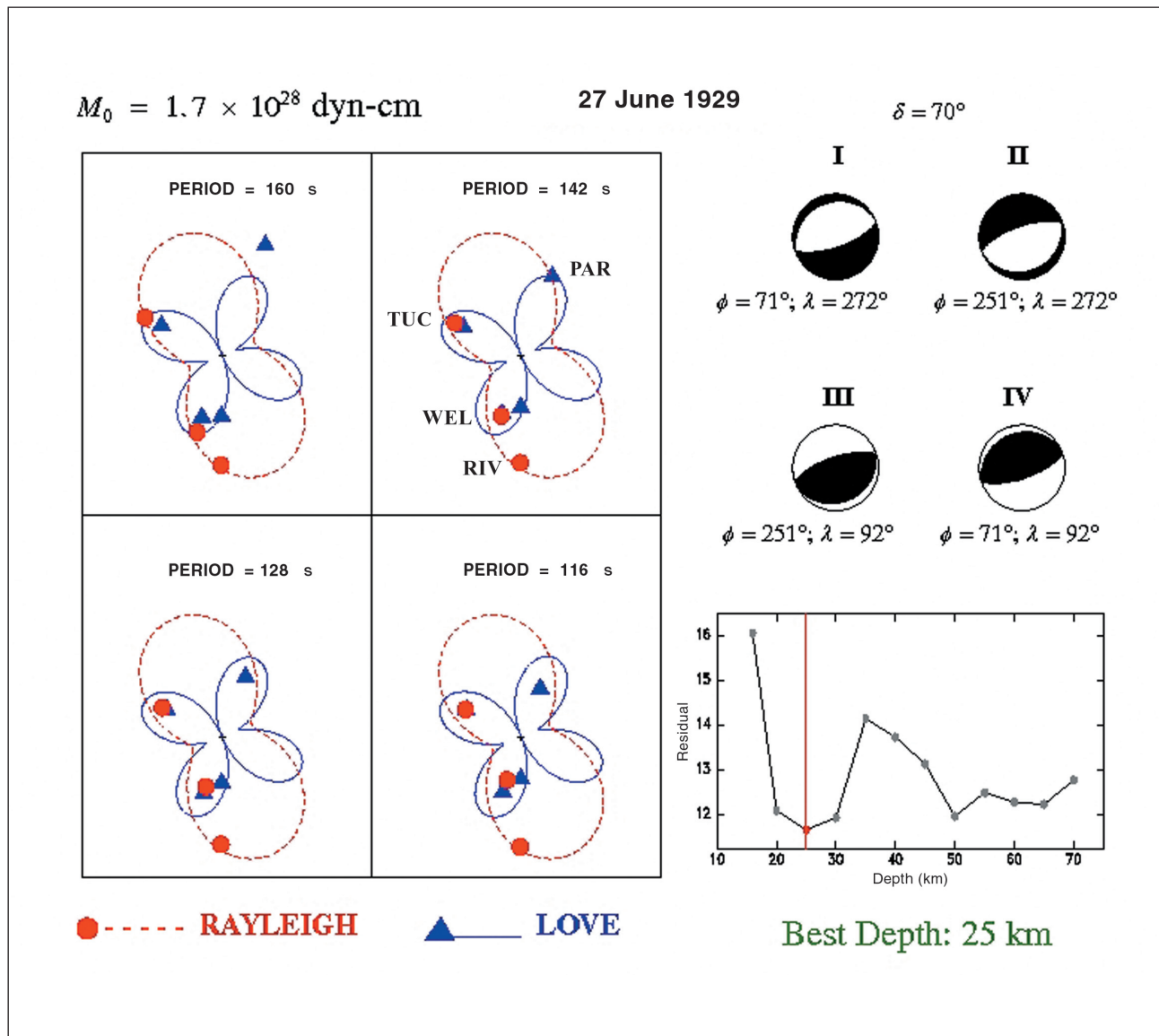
The simulation is carried out on a grid covering the entire South Atlantic and Indian Oceans, with a step of 0.1° (11.12 km in latitude, but as little as 3.8 km in longitude at its southern border). This rather coarse grid does not allow run-up computations for individual beaches or harbours; this would require a finer grid for both bathymetry and topography (with a sampling down to a few tens of meters), which is beyond the scope of this paper. In this respect, our simulations do not pretend to predict run-up at individual sites, but rather to present regional trends in the amplitude of the deep

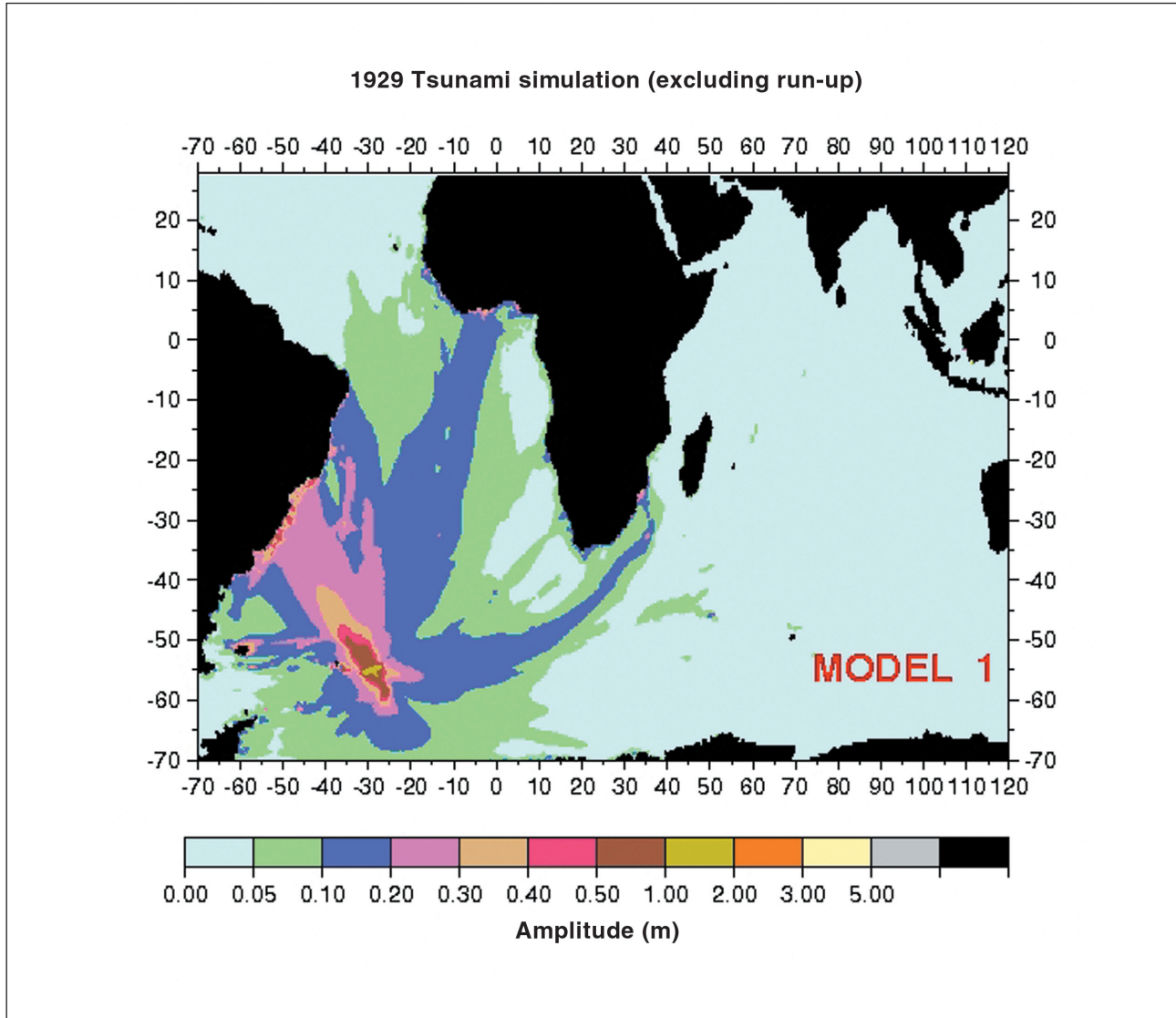water waves, which could be used as initial conditions for more detailed modeling.

The time step, δt = 15 s, is taken to satisfy the classical stability conditions of Courant, Friedrichs and Lewy (1928), even at the highest latitudes; the simulation is carried out for a total of 5000 steps (20.8 hours) and saved every 60 steps or 15 minutes.

Figure 5 shows the results, expressed as the field of maximum amplitudes over time $\eta_{max}\,(x,\,y)$ for each grid point. It is clear that the far-field amplitudes are dominated by two effects. First, source directivity is expressed by a strong lobe at right angles to the direction of rupture, in application of Ben-Menahem and Rosenman's (1972) classical concept, resulting in

particularly strong amplitudes in deep water offshore of Brazil. Second, shallow bathymetry results in focusing effects due to refraction caused by the dependence of tsunami phase velocity on depth ($C = (g\,H)^{1/2}$)(Woods and Okal, 1987; Satake, 1988). In the present geometry, these effects are strong and continuous along the South Atlantic Mid-Oceanic Ridge, delivering strong amplitudes into the Gulf of Guinea, principally offshore of Ghana and the Ivory Coast, and also along the Southwest Indian Ocean Ridge and its bathymetric offshoots, the Agulhas and Mozambique plateaux, resulting in focusing of the wave energy towards certain segments of the coastlines of South Africa and southern Mozambique.

Figure 4. *Results of the PDFM inversion. Left: Azimuthal fits of inverted spectra at the four stations used, for a representative set of periods. The solid (Love) and dashed (Rayleigh) lines are the theoretical spectral amplitudes, the dots (Rayleigh) and triangles (Love), the observed values. The scale is common in each box, but vary with period. Top right: Sketch of the four possible focal mechanisms corresponding to the inverted solution. Bottom right: Variation with source depth of the inversion residual (solid line and dots; in arbitrary units). Its minimum around 25 km is interpreted as the centroid of rupture.*

Figure 5. *Results of the tsunami simulation for the 1929 preferred source. This figure plots the maximum amplitude of the vertical displacement of the ocean surface,* η_{max} *(x, y), using the parameters listed as "Model 1" in Table 3.*
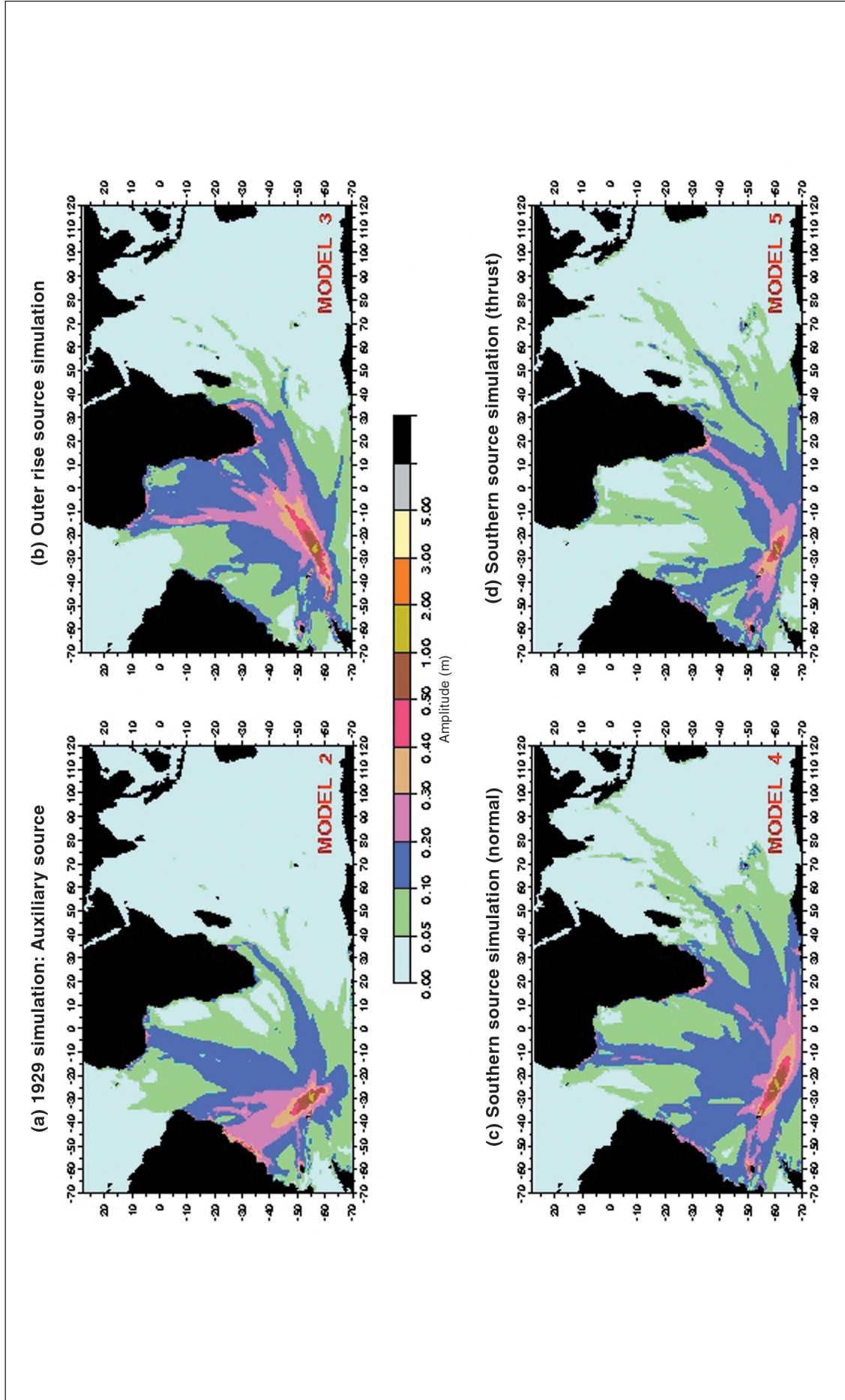
The simulation in Figure 5 was run using the preferred focal mechanism derived from the PDFM inversion (φ=71°; δ=70°; λ = 272°). We verified that the use of the conjugate solution (Model 2 in Table 3; φ=245°; δ=20°; λ = 265°) leaves the far field of the tsunami essentially unaffected, with differences in maximum amplitudes remaining below 5 cm in the deep water offshore of the coastlines involved (Figure 6a).

Table 3. Parameters used for tsunami simulation

Number	Model	Moment	Fault Length	Fault Width	Slip	Focal Mechanism			Source Location		
						Strike φ	Dip δ	Slip λ	Latitude	Longitude	Depth (†)
		(10^{27} dyn.cm)	(km)	(km)	(m)	(°)	(°)	(°)	(°S)	(°W)	(km)
1	1929 Preferred	17	133	66	3.9	71	70	272	54.5	29.5	15
2	1929 Auxiliary Plane	17	133	66	3.9	245	20	265	54.5	29.5	15
3	Outer Rise Scenario	17	133	66	3.9	322	31	272	56	24.5	15
4	Southern Normal Scenario	17	133	66	3.9	231	35	278	60.3	24.2	15
5	Southern Thrust Scenario	17	133	66	3.9	232	16	123	60.3	26.9	15

† The depth is taken at the top of the fault area.

Figure 6. *Same as Figure 5 in the case of (**a**) the 1929 earthquake, using the auxiliary fault plane (Model 2); (**b**) an event with the geometry of the outer rise earthquake of 1991 (Model 3); (**c**) a normal faulting event in the geometry of the 1983 earthquake at the southern corner of the arc (Model 4); and (**d**) an event in the geometry of the interplate earthquake of 1987 at a nearby location (Model 5). See the text and Table 3 for details. All models share the scalar moment of the 1929 event as resulting from the PDFM inversion.*

In addition, we explored the far-field tsunamis generated by other potential seismic sources in the South Sandwich area. We consider the sites of modern large earthquakes with published CMT solutions: the outer rise normal faulting event of 27 December 1991, the interplate thrust earthquake of 30 January 1987 at the extreme southern end of the arc, and the nearby normal faulting event of 22 October 1983, whose epicenters are shown on Figure 2a. For each of them, we retain its location and focal mechanism, but boost the seismic moment to the value inverted for the 1929 shock (1.7 x 10^{28} dyn.cm). While this choice may seem arbitrary, it reflects the occasional occurrence of normal faulting outer rise events at even greater moments, such as the Showa Sanriku earthquake of 1933 (M_0 = 4.3 x 10^{28} dyn.cm (Kanamori, 1971)), whose tsunami, catastrophic in the near field, remained substantial in the far field, with run-up reaching 3 m in Hawaii and 1.1 m in Crescent City, California; the size of that earthquake remains unique in the instrumental record, suggesting that the era of modern seismological instrumentation may significantly undersample large normal faulting events in other seismic provinces, and thus justifying Models 3 and 4. As for Model 5, it considers an interplate thrust event at the southern tip of the arc, in the vicinity of the documented earthquake of 1983, and also of a large shock (M_{PAS} = 7.3) which took place on 25 March 1943.

The results of these additional simulations are shown on Figure 6b, c, d. Predictably, the change in fault azimuth results in a rotation of the lobe of directivity and consequently in much smaller amplitudes along the South American coast, while greater ones are predicted along the whole Atlantic shoreline of Africa, particularly in Namibia and South Africa. This effect is particularly strong under Scenario 3. In addition, the focusing effects due to shallow bathymetry along the ridges are unchanged, and thus significant amplitudes are found from Guinea to Ivory Coast and in southern Mozambique, especially under Scenario 3.

In conclusion of this section, we establish that the South Sandwich subduction zone bears significant tsunami hazard for the coastlines of the South Atlantic. Our simulations suggest that the 1929 earthquake generated a tsunami whose deep water amplitude reached ~30 cm off the shore of Brazil, and 20 cm off the coastlines of Ghana and southern Mozambique. While definitive run-up predictions at individual sites are beyond the scope of this paper as they require detailed bathymetry and topography, such amplitudes would almost certainly have resulted in detectable, and possibly damaging, effects along the relevant coastlines. Unfortunately, and because of the scarcity of historical data, we have not been able to confirm or refute these predictions (for example, there are no tidal gauge records archived in South Africa for this period of time).

Discussion and conclusion

In attempting to estimate tsunami risk from the South Sandwich province, we note that the question of the maximum size of interplate earthquakes at subduction zones was reopened in the wake of the 2004 Sumatra earthquake. Stein and Okal (2007) noticed that the size of that earthquake was in defiance of the maximum predicted by Ruff and Kanamori's (1980) model for the relevant combination of lithospheric age and convergence rate, and went along to point out that an updated dataset of such tectonic parameters led to a degradation of the correlation between observed maximum earthquake size and that predicted by Ruff and Kanamori's paradigm. Indeed, the case of the SSI arc would appear as a flagrant one of "false alarm", since its relatively young age (40 Ma on the average) and fast rate (78 mm/yr) would predict events reaching 10^{29} dyn.cm (assuming a long enough fault zone), whereas the largest documented interplate thrust event (the 1987 earthquake on Figure 2a) remains less than 10^{27} dyn.cm. However, we caution against a rapid conclusion since the lack of documented larger earthquakes may simply be an artifact of insufficient time sampling, as was the case of the 1700 Cascadia earthquake (essentially unsuspected until the work of Satake et al. (1996)). In this respect, further study of the earthquakes of 09 and 25 March 1943 at the Southern corner of the arc, and of 02 November 1943 in its northern section, all of which were assigned magnitudes of 7.2 or 7.3 by Gutenberg and Richter (1954), would be desirable.

However, the main tsunami risk in SSI may take the form of normal faulting earthquakes. Our study has shown that the event of 27 June 1929, which relocates outside the plate boundary as expressed by the belt of modern seismicity, features normal faulting and can be interpreted as involving a tear of the South American plate at the north-eastern corner of the arc, in a geometry reminiscent of processes observed at several other subduction zones. With a seismic moment of 1.7 x 10^{28} dyn.cm, we confirm that the 1929 earthquake was indeed a major event, most probably the largest one recorded in the region since the dawn of instrumental seismology. It is comparable in size to other large normal faulting earthquakes which have occurred in the vicinity of subduction zones, but not at the plate interface (e.g., Indonesia, 1977; Sanriku, 1933; Aleutian, 1929). Such events can generate significant tsunamis and since they can occur in subduction zones apparently deprived of large interplate earthquakes, they represent the major contributor to tsunami risk in such environments; this would in particular include the Marianas and Vanuatu arcs. Unfortunately, little if anything is known of their possible recurrence rates, and it is clear that detailed seismological studies of historical earthquakes of this type will be required if we are to achieve some understanding of the tsunami risk from the relevant seismic provinces.

The most intriguing result of our study is the realisation that Brazil on the one hand, and the shoreline extending from Guinea to Cameroon on the other, could be threatened by tsunamis generated by large SSI earthquakes, the former under a source geometry similar to that of the 1929 earthquake; the latter under several scenarios (primarily a large outer rise event) on account of the systematic focusing of tsunami energy by the south Atlantic Ridge, a well-known phenomenon observed along the southwest Indian Ocean Ridge during the 2004 Sumatra tsunami (Titov et al., 2005).

In the particular case of the exposure of South Africa to tsunamis from the SSI, our simulations (and in particular the comparison of Figures 6c and d) suggest that the offshore amplitude attacking South Africa results from a subtle combination of the effects of source directivity and focusing during propagation. The most dangerous scenarios are an outer rise event (Number 3) from the centre of the arc, and an interplate thrust from its southern corner (Number 5). Both types of events are documented in the modern record, albeit at a much reduced size; our study shows that the required size is documented (the 1929 event), albeit in a geometry benign for South Africa. Even if its probability (that we do not know how to compute, since we ignore the recurrence rates of intraplate events) can be assumed to be low, there is no reason, in our opinion, to refute the possibility of an SSI event combining the two requirements and generating a tsunami which could be destructive in South Africa.

Acknowledgments

References

Abe, K. (1972). Focal process of the South Sandwich Islands earthquake of May 26, 1964, *Physics of the Earth and Planetary Interiors*, **5**, 110–122.

Alvarez, W. (1982). Geological evidence for the geographical pattern of mantle return flow and the driving mechanism of plate tectonics, *Journal of Geophysical Research,* **87**, 6697–6710.

Baker, P.E. (1990). South Sandwich Islands. *In:* W.E. LeMasurier and J.W. Thompson (Editors), Volcanoes of the Antarctic Plate and Southern Oceans, Antarctic Research Series, **48**, *American Geophysical Union, Washington, D.C., United States of America*, 360–396.

Barker, P.F. (1972). A spreading center in the East Scotia Sea, *Earth and Planetary Science Letters*, **15**, 123–132.

Ben-Menahem, A. and Rosenman, M. (1972). Amplitude patterns of tsunami waves from submarine earthquakes, *Journal of Geophysical Research*, **77**, 3097–3128.

Bernard, P. and Zollo, A. (1989). The Irpinia (Italy) 1980 earthquake: Detailed analysis of a complex normal faulting earthquake, *Journal of Geophysical Research*, **94**, 1631–1647.

Courant, R., Friedrichs, K. and Lewy, H. (1928). Über die partiellen Differenzengleichungen der mathematischen Physik, *Mathematische Annalen,* **100**, 32–74.

Engdahl, E.R. and Villaseñor, A. (2002). Global Seismicity: 1900-1999. *In:* W.H.K. Lee, H. Kanamori, P.C. Jennings and C. Kisslinger (Editors). International Handbook of Earthquake and Engineering Seismology, Part A, Chapter 41, *Academic Press, San Diego, United States of America*, 665–690.

Forsyth, D.W. (1975). Fault plane solutions and tectonics of the South Atlantic and Scotia Sea, *Journal of Geophysical Research*, **80**, 1429–1443.

Geller, R.J. (1976). Scaling relations for earthquake source parameters and magnitudes, *Bulletin of the Seismological Society of America*, **66**, 1501–1523.

Godunov, S.K. (1959). Finite difference methods for numerical computations of discontinuous solutions of the equations of fluid dynamics, *Matemat. Sbornik*, **47**, 271–295.

Govers, R. and Wortel. M.J.R. (2005). Lithosphere tearing at STEP faults: Response to edges of subduction zones, *Earth and Planetary Science Letters*, **236**, 505–523.

Gutenberg, B. and Richter, C.F. (1954). Seismicity of the Earth and associated phenomena. *Princeton University Press., Princeton, United States of America,* 310pp.

Hartnady, C.J.H. and Okal, E.A. (2008). Mentawai tsunami effect at Port Elizabeth, South Africa on 12-14 September 2007, *South African Journal of Science,* (submitted).

Holdgate, M.W. and Baker, P.E. (1979). *The South Sandwich Islands, I, General description*, British Antarctic Survey Science Report, **91**, 76pp.

Isacks, B.L., Sykes, L.R. and Oliver, J.E. (1969). Focal mechanisms of deep and shallow earthquakes in the Tonga-Kermadec region and the tectonics of island arcs, *Geological Society of America Bulletin*, **80**, 1443–1469.

Kanamori, H. (1971). Seismological evidence for a lithospheric normal faulting – The Sanriku earthquake of 1933, *Physics of the Earth and Planetary Interiors*, **4**, 289–300.

Larson, R.L., Pitman III, W.C., Golovchneko, X., Cande, S.C., Dewey, J.F., Haxby, W.F. and LaBrecque, L.L. (1985). The Bedrock Geology of the World*, W.H. Freeman and Co., New York, United States of America*, Map.

Mansinha, L. and Smylie, D.E. (1971). The displacement fields of inclined faults, *Bulletin of the Seismological Society of America*, **61**, 1433–1440.

Millen, D.W. and Hamburger, M.W. (1998). Seismological evidence for tearing of the Pacific plate at the Northern termination of the Tonga subduction zone, *Geology,* **26**, 659–662.

Okal, E.A. (1992). Use of the mantle magnitude M_m for the reassessment of the seismic moment of historical earthquakes. II. Intermediate and deep events, *Pure and Applied Geophysics,* **139**, 59–85.

Okal, E.A. (2005). A re-evaluation of the great Aleutian and Chilean earthquakes of 1906 August 17, *Geophysical Journal International,* **161**, 268–282.

Okal, E.A. and D. Reymond (2003). The mechanism of the great Banda Sea earthquake of 01 February 1938: Applying the method of Preliminary Determination of Focal Mechanism to a historical event, *Earth and Planetary Science Letters*, **216**, 1–15.

Okal, E.A. and Synolakis, C.E. (2008). Far-field tsunami hazard from megathrust earthquakes in the Indian Ocean, *Geophysical Journal International*, **172**, 995–1015.

Okal, E.A. and Talandier, J. (1989). M_m : A variable period mantle magnitude, *Journal of Geophysical Research*, **94**, 4169–4193.

Pelletier, B., Calmant, S. and Pillet, R. (1998). Current tectonics of the Tonga-New Hebrides region, *Earth and Planetary Science Letters*, **164**, 263–273.

Reymond, D. and Okal, E.A. (2000). Preliminary determination of focal mechanisms from the inversion of spectral amplitudes of mantle waves, *Physics of the Earth and Planetary Interiors*, **121**, 249–271.

Romanowicz, B.A. and Suárez, G. (1983). An improved method to obtain the moment tensor depth of earthquakes from the amplitude spectrum of Rayleigh waves, *Bulletin of the Seismological Society of America*, **73**, 1513–1526.

Ruff, L.J. and Kanamori, H. (1980). Seismicity and the subduction process, *Physics of the Earth and Planetary Interiors*, **23**, 240–252.

Russo, R.M. and Silver, P.G. (1996). Cordillera formation, mantle dynamics, and the Wilson cycle, *Geology*, **24**, 511–514.

Satake, K. (1988). Effects of bathymetry on tsunami propagation: Application of ray tracing to tsunamis, *Pure and Applied Geophysics,* **126**, 27–36.

Satake, K., Shimazaki, K. Tsuji, Y. and Ueda, K. (1996). Time and size of a giant earthquake in Cascadia inferred from Japanese tsunami records of January 1700, *Nature,* **379**, 246–249.

Sclater, J.G., Bowin, C., Hey, R., Hoskins, H. Peirce, J., Phillips, J. and Tapscott, C. (1976). The Bouvet triple junction, *Journal of Geophysical Research,* **81**, 1857–1869.

Stein, S. and Okal, E.A. (2007). Ultra-long period seismic study of the December 2004 Indian Ocean earthquake and implications for regional tectonics and the subduction process, *Bulletin of the Seismological Society of America*, **97**, S279–S295.

Synolakis, C.E. (2002). Tsunami and seiche. *In:* W.-F. Chen and C. Scawthron (Editors). Earthquake Engineering Handbook, *CRC Press, Boca Raton, United States of America*, **9**, 1–9.

Thomas, C., Livermore, R. and Pollitz, F. (2003). Motion of the Scotia Sea plates, *Geophysical Journal International*, **155**, 789–804.

Titov, V.V. and Synolakis, C.E. (1998). Numerical modeling of tidal wave runup, *Journal of Waterway, Port, Coastal, and Ocean Engineering*, **124**, 157–171.

Titov, V.V., Rabinovich, A.B., Mofjed, H.O., Thomson, R.E. and González, F.I. (2005). The global reach of the 26 December 2004 Sumatra tsunami, *Science,* **309**, 2045–2048.

Wessel, P. and Smith, W.H.F (1991). Free software helps map and display data, *Eos, Transactions of the American Geophysical Union*, **72**, 441 and 445–446.

Wilson, J.T. (1966). Are the structures of the Caribbean and Scotia Arc regions analogous to ice rafting? *Earth and Planetary Science Letters*, **1**, 335–338.

Woods, M.T. and Okal, E.A. (1987). Effect of variable bathymetry on the amplitude of teleseismic tsunamis: a ray-tracing experiment, *Geophysical Research Letters,* **14**, 765–768.

Wysession, M.E., Okal, E.A. and Miller, K.L. (1991). Intraplate seismicity of the Pacific Basin, 1913-1988, *Pure and Applied Geophysics,* **135**, 261–359.